Chapter

Growth of Single-Crystal $LiNbO_3$ Particles by Aerosol-Assisted Chemical Vapor Deposition Method

José G. Murillo, José A. Ocón, Guillermo M. Herrera, José R. Murillo-Ochoa and Gabriela Ocón

Abstract

Adjusting nucleation conditions, an effective shape and size control in the preparation of single-crystal lithium niobate nanoparticles by aerosol-assisted chemical vapor deposition method was demonstrated. The effect of the most relevant parameters leading to nanocrystals taking a specific shape or size once they are synthesized was analyzed. This has allowed us to demonstrate that it is possible to control the size and morphology of particles prepared adjusting the nucleation conditions. The synthesized nanocrystals showed different morphologies including quasi-cubic, tetrahedral, polyhedral, and hexagonal shapes, with characteristic sizes ranging from a few tens to a few hundred nanometers. However, rod-like structures with characteristic lengths ranging from 3 to 5 μm were also obtained. The structural and morphological characterization by X-ray diffraction and high-resolution electron microscopy techniques revealed the single-crystal nature of the synthesized particles.

Keywords: $LiNbO_3$ nanocrystals, aerosol-assisted chemical vapor deposition, nanomaterials, niobates, ferroelectric materials

1. Introduction

Lithium niobate ($LiNbO_3$) has been one of the most prominent and widely studied ferroelectric materials in the last decades. Their extraordinary pyroelectric, piezoelectric, and strong nonlinear optical properties have turned it into a key material in photonics and integrated optics [1–4]. The diverse, large-magnitude physical properties of $LiNbO_3$ (LN) have allowed it to be used in information storage and processing [5], in optical channel waveguides [6, 7], and in electro-optical modulation [8].

Moreover, in the last decade, a great interest has arisen for the synthesis of nanosized LN, including nanowires and nanoparticles [9–15]. This growing interest in the synthesis of nanoscale materials is originated by their new properties with potential technological application arising from the dimensional confinement [16, 17]. In view of that, in this research we describe in detail the synthesis and the

morphological and structural characterization of LN nanoparticles using high-resolution electron microscopy techniques.

To obtain LN particles, several synthesis routes have been reported in literature, which have resulted in different shapes, sizes, and degree of crystallinity. Flake-shaped LN nanocrystals with 40–100 nm in diameter and LN anisotropic nanorods with lengths up to 100 and 7 nm diameters have already been obtained by hydrothermal route and by solution-phase synthesis [18–20]. By coprecipitation method LN particles have been synthesized with a loosely porous packed shape [21]. Furthermore, using sol-gel method, powders that after thermal treatment present the crystalline phase of LN with sizes lower than 100 nm and a roughly spherical geometry have been synthesized [22]. Under solvothermal conditions cubic and sphere-like LN nanoparticles have been prepared [23]. Nevertheless, there are still some important challenges to be solved such as growth direction, size and shape control, and degree of crystallinity.

The aim of this research is to describe in detail the synthesis process of LN nanocrystals, to present their morphology and structural characteristics, and also to demonstrate that it is possible to control the size and morphology of LN nanocrystals synthesized by the aerosol-assisted chemical vapor deposition method (AACVD). We describe a detailed characterization of the LN particles synthesized, including an analysis of the nucleation conditions that allow the control of their size and morphology. We have analyzed the effect of the most relevant parameters leading to the nanocrystals taking a specific shape or size when synthesized by the AACVD method. It was observed that depending on the exact conditions of the synthesis process, nanocrystals showed different morphologies including quasi-cubic, tetrahedral, polyhedral, and hexagonal shapes, with characteristic sizes ranging from a few tens to a few hundred nanometers or even rod-like particles with characteristic lengths ranging from 3 to 5 μm. The nanocrystals prepared were characterized by grazing incidence X-ray diffraction (GIXRD), scanning electron microscopy (SEM), and high-resolution transmission electron microscopy (HRTEM).

2. Experimental procedure

The LN nanocrystals were prepared following the same procedure used to obtain a thin film by the AACVD method as described in Refs. [24, 25]. That is, a silicon (0 0 1) or sapphire (1 1 0) substrate (1.5 × 1.5 cm^2) was used as a support medium for nanoparticle growth. In the LN nanoparticles' synthesis process, the determination of the deposition conditions was based on the route used in Ref. [26] to prepare a LN thin film. Nevertheless, some of the nucleation conditions useful for growing LN thin films were modified or optimized to obtain LN nanocrystals. Silicon was selected as substrate in order to combine its electronic advantages with the LN piezoelectric properties and optical processing capabilities. Concerning the sapphire substrate, its lattice parameters similar to LN enable the hetero-epitaxial growth of LN piezoelectric particles, i.e., with their atomic planes built following the same crystallographic orientation of the atomic planes on the substrate surface [26].

In order to evaluate possible changes in the crystalline structure, size, and morphological characteristics of the LN particles synthesized, two deposition systems were used, one with a fixed and the other with a mobile nozzle. In both cases the nozzle discharge surface was 1 mm × 150 mm.

The fixed nozzle deposition system uses an ultrasonic nebulizer working at 2.4 MHz to generate the aerosol precursor solution which is conveyed by a carrier gas (dry and clean air) and directed toward the substrate by the nozzle. The

substrate is directly in contact with a metallic plate heated at the selected temperature. The general properties and details of the deposition systems are published elsewhere [25]. The nanocrystals were prepared at different temperatures covering the range from 653 to 783 K. In order to determine the optimal conditions to obtain LN nanocrystals keeping control of the size and shape, we also varied the carrier gas flow, the nozzle-to-substrate distance, and deposition time. The other deposition system is very similar to the system described above, except for the use of a mobile nozzle which describes a back-and-forth movement at constant velocity (~ 1 cm min^{-1}) to scan the whole surface of the substrate. By varying the total number of scans, we obtained particles of different sizes. The starting solutions for feeding the ultrasonic nebulizer which generates the aerosol precursor were dilutions of niobium ethoxide (99.95% Sigma-Aldrich) and lithium acetylacetonate (97% Sigma-Aldrich) in methanol or ethanol, using concentrations from 0.01 to 0.1 mol l^{-1}.

The morphological and structural characterization of the LN nanocrystals obtained was completed by GIXRD, SEM, and HRTEM. The crystalline phases present in nanoparticles were determined by GIXRD patterns in a Panalytical X-Pert system using Cu Kα radiation ($\lambda = 0.15418$ nm) at 40 keV and 35 mA. The grazing incidence angle was fixed at 0.5°, and the scanning angle 2θ was varied from 20 to 80° at 0.1°min^{-1} intervals. The surface morphology was studied by field emission SEM using a JEOL JSM-7401F operated at 2 kV.

3. Results and discussion

3.1 Synthesis

We accomplished a systematic variation of the nucleation conditions used in nanocrystals growth process, including substrate type and temperature, carrier gas flux of the precursor aerosol, nozzle-to-substrate distance, and solvent type (methanol or ethanol) used to prepare the precursor solution.

The LN nanocrystals obtained showed different sizes and morphologies including multifaceted shapes, quasi-cubic shapes, tetrahedral shapes, diamond-like polyhedrons, hexagonal prism shapes, or hexagonal rod-like shapes depending on the exact nucleation conditions used in the synthesis process. In fact, a large number of deposition cycles were carried out by AACVD method on silicon (0 0 1) or sapphire (1 1 0) substrates, to investigate the possibility of obtaining LN particles with different shapes and sizes. Some representative LN structures synthesized on silicon or sapphire substrates with both the fixed nozzle system and the mobile nozzle system are shown below. **Figure 1(a)–(c)** shows SEM micrographs describing the morphology of some typical LN nanocrystals obtained using ethanol as solvent in the precursor solution. **Figure 1(d)–(h)** shows SEM micrographs of the morphology of some LN nanocrystals obtained dissolving precursor solution in methanol.

3.2 Morphological and structural characterization

It was found from a detailed analysis of the controlled nucleation conditions used in the crystalline structure growth process that substrate temperature is a particularly crucial parameter in the synthesis process. The optimal temperature range required to obtain LN crystals with faceted shapes was 653–783 K. Temperatures out of this range caused the formation of non-faceted particles with rock-like or island-like shapes similar to a piece of thin film. The carrier gas flow magnitude was also decisive in the shape of LN crystals. Indeed, fluxes between 5 and 6 l/min led to the

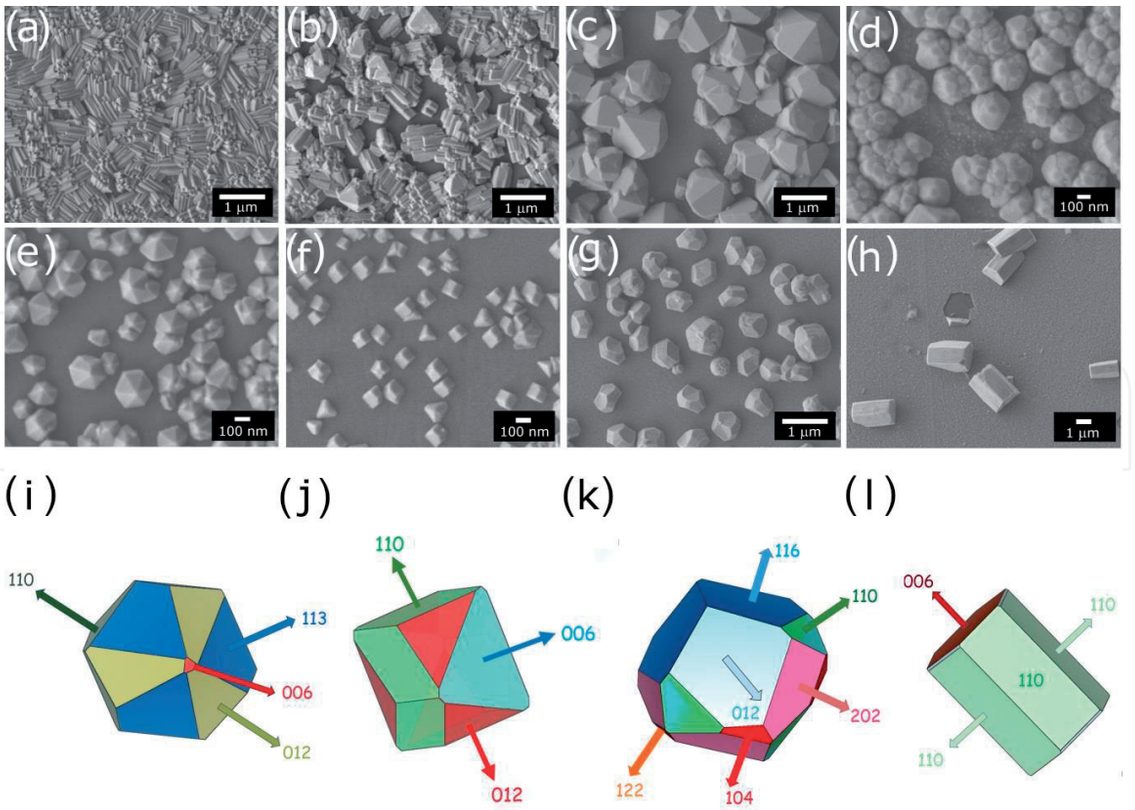

Figure 1.
(a)–(c) Typical LN nanocrystals obtained using ethanol as solvent in the precursor solution, and prepared on a Si substrate, (a) and (b) rod-like type I particles, (c) polyhedral type II particles. (d)-(h) Representative LN nanocrystals obtained dissolving the precursor solution in methanol. (d), (e), (g) and (h) prepared on a (001) Si substrate, and (f) on a (1 1 0) sapphire substrate. (d) Agglomerated polyhedral type III particles, (e) diamond-like polyhedral type IV particles, (f) a mix of quasi-cubic type V and tetrahedral type VI nanoparticles, (g) polyhedral type VII particles, and (h) hexagonal prism type VIII particles. (i), (j), (k) and (l) particles morphology showing the crystallographic orientation of the facets in selected particles of representative samples LN73S, LN37SP, LN53S and LN128S shown in Figure (e), (f), (g) and (h), respectively, reproduced using the software VESTA[29] simulated according to the texture observed in the corresponding GIXRD results.

formation of rod-like particles (**Figure 1(a)** and **(b)**), while fluxes between 2 and 3 l/min led to faceted particles with polyhedral morphology or diamond-like shape (**Figure 1(e)–(g)**). The molar concentration of the precursors diluted in methanol or ethanol also had an important effect on the LN crystal shape and size. The use of low molar precursor concentrations in the solution to be sprayed of the order of 0.01–0.02 mol l^{-1} led to the formation of polyhedral diamond-like particles at 773 K (**Figure 1(e)**), hexagonal prism shapes at 653 K (**Figure 1(h)**), or quasi-cubic shapes if the substrate is sapphire instead of silicon at 723 K (**Figure 1(f)**).

On the other hand, the use of methanol or ethanol as solvent in the precursor solution used in the synthesis process had a strong effect on the determination of LN particle morphology. This finding is in agreement with the results reported in Ref. [27] where the great influence of alcohols used as solvents on the morphology and size of iron oxide nanoparticles synthesized by sol–gel method is evinced. As shown in **Figure 1**, we obtained rod-like type I particles (**Figure 1(a)–(b)** samples LN11S and LN12S), polyhedral type II particles (**Figure 1(c)** sample LN30S), agglomerated polyhedral shape type III particles (**Figure 1(d)** sample LN77S), polyhedral diamond-like type IV particles (**Figure 1(e)** sample LN73S), quasi-cubic type V and tetrahedral type VI particles (**Figure 1(f)** sample LN37SP), polyhedral type VII particles (**Figure 1(g)** sample LN53S), or even hexagonal prism type VIII particles (**Figure 1(h)** sample LN128S). Specifically, it was found that the use of

methanol to dilute the precursor solution enables the formation of polyhedral type III, diamond-like polyhedral (type IV), quasi-cubic type V, tetrahedral type VI, and polyhedral type VII particles at the adequate temperature (653–773 K) (**Figure 1(d)–(g)**). However, the use of ethanol as solvent in the precursor solution enables the formation of extended rod-like particles and polyhedral type II particles, using the fixed nozzle deposition system (**Figure 1(a)–(c)**). Nevertheless, using methanol in the dilution of precursor and the mobile nozzle system, it is also possible to obtain hexagonal prism type VIII particles (**Figure 1(h)**). In addition to this, the specific characteristics of the synthesized LN particles also depended on the specific deposition system used. The fixed nozzle deposition system enables the production of rod-like particles (**Figure 1(a)–(b)**) and polyhedral type II particles (**Figure 1(c)**), due to the high amount of material sprayed into the substrate. In contrast, the mobile nozzle system enables the production of polyhedral and diamond-like particles (**Figure 1(c)–(e)**). Moreover, in **Figure 1(f)** it can be observed that it is possible to produce particles with quasi-cubic and tetrahedral morphologies, keeping the nucleation parameters close to the required values and changing only the type of substrate. It is clear then that the substrate crystallographic orientation plays an important role in the resultant morphology of synthesized LN particles, since the crystallographic orientation of the sapphire substrate (1 1 0) was different to that of the silicon substrate (0 0 1) used. LN particles in sample LN37SP (**Figure 1(f)**) were synthesized on a sapphire substrate using a set of nucleation parameters very similar to those used to produce the particles in sample LN53S (**Figure 1(g)**). Furthermore, it was observed that under certain nucleation conditions, the synthesis of nanocrystals could finish in a continuous layer or thin film. **Figure 1(h)** shows six very large LN hexagonal structures over a continuous LN thin film obtained at a temperature of 653 K with the mobile nozzle system, using a carrier gas flow of 1 l/min, and a deposition time of 130 min. **Figure 1(i)–(l)** shows the particle morphology of samples LN73S, LN37SP, LN53S, and LN128S shown, respectively, in **Figure 1(e)–(h)** reproduced using the software VESTA [28] that additionally allowed us to determine the crystallographic orientation of these particle facets. The crystallographic facets of the particles in these figures were simulated according to the texture observed in their corresponding GIXRD results. **Table 1** summarizes the nucleation conditions used to obtain some of the representative LN particles studied in this work.

The crystalline nature of some of the representative particles was verified from its GIXRD pattern. **Figure 2(a)–(d)** shows the comparison between GIXRD patterns for samples prepared with methanol labeled as LN53S, LN37SP, and LN73S with respect to the sample prepared with ethanol labeled as LN11S. The crystalline structure for these GIXRD patterns was related to lithium niobate, and the diffraction peaks were indexed through the JCPD 01-070-8451 file [29]. These results correspond to a rhombohedral phase with a R3c (161) space group. Other diffraction peaks labeled with asterisk correspond to the Si substrate, JCPD 00-027-1402, and those with a cross to the sapphire substrate, JCPD 00-001-1305 [29]. The GIXRD pattern for the samples prepared with methanol showed two diffraction peaks denoted by (012) and (104). This result suggests the presence of a preferred growth orientation (texture) with respect to the sample which was prepared with ethanol. The presence of texture in sample LN73S prepared with methanol could be attributed to a combination of synthesis parameters during the sample preparation such as temperature, molar concentration, growth time, type of solvent, fixed or mobile nozzle system, air flux, etc. Furthermore, it can be seen in **Figure 2(c)** that the diffraction peaks in the GIXRD pattern in sample LN73S show a sharper and narrower profile than the diffraction peaks in the GIXRD pattern of sample LN11S shown in **Figure 2(d)**.

Sample	Substrate	Solvent	Precursor concentration (mol/l)	Substrate temperature (K)	Carrier gas flow (l/min)	Nozzle system	Scanning rate system (cm/min)	Growth time (min)
LN11S	Silicon	Ethanol	0.1	783	5	Fixed	—	30
LN12S	Silicon	Ethanol	0.1	773	5	Fixed	—	30
LN30S	Silicon	Ethanol	0.05	773	5	Mobile	0.2	120
LN37SP	Sapphire	Methanol	0.02	723	2	Fixed	—	60
LN53S	Silicon	Methanol	0.02	723	2	Fixed	—	120
LN73S	Silicon	Methanol	0.02	723	3	Mobile	1	60
LN77S	Silicon	Methanol	0.01	773	3	Mobile	1	40
LN128S	Silicon	Methanol	0.01	653	1	Mobile	1	130

Table 1.
Nucleation conditions used to synthesize representative LN particles.

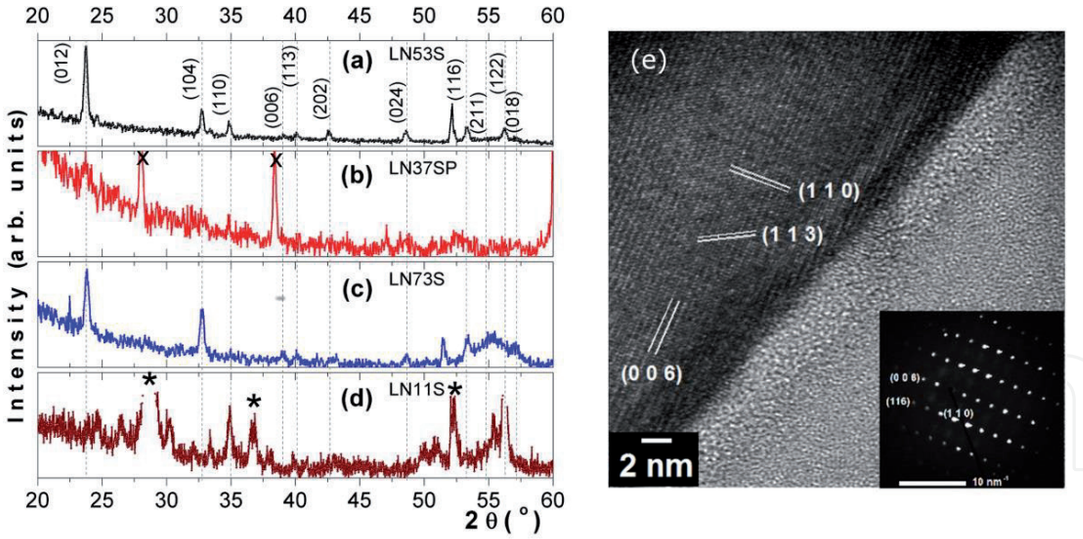

Figure 2.
Comparison between GIXRD patterns for samples prepared with methanol labeled as (a) LN53C, (b) LN37SP, and (c) LN73S, respect to the sample prepared with ethanol labeled as (d) LN11S, other diffraction peaks labeled with asterisk correspond to the Si substrate and those with a cross to the sapphire substrate. (e) Bright field HRTM image of the interface between a LN nanocrystal such as shown in ***Figure 1(e)*** *and a Si substrate showing the interplanar distance of the (0 0 6), (1 1 0) and (1 1 3) family planes of the lithium niobate hexagonal phase. In the lower half of the micrograph is shown a sharp interface between a $LiNbO_3$ nanocrystal and an amorphous native thin silicon oxide interlayer. The inset in the lower right corner shows a selected area electron diffraction pattern demonstrating the existence of the single crystal hexagonal phase.*

In order to determine the particle mean crystal size in sample LN73S, we used the Scherrer equation:

$$C = 0.9\,\lambda/\beta\cos\theta \qquad (1)$$

where C is the mean crystal size, λ is the wavelength of CuKα (1.54 Å), β is the full width half maximum (FWHM) intensity corrected using LaB6 as the standard, and θ is Bragg's angle of the selected peaks (=23.79 and 32.81°). The mean crystal size for particle in LN73S sample was 33.9 nm which matches the dimensions shown in the morphology micrographs evaluated by SEM.

GIXRD results were confirmed by HRTEM techniques preparing first a sample with a cross-section of some LN nanocrystals as those shown in **Figure 1(e)**. **Figure 2(e)** shows a bright-field high-resolution TEM image of the interface between the Si substrate and a LN nanocrystal. The lattice fringe measurement (**Figure 2(e)**) was consistent with the interplanar distance of the (0 0 6), (1 1 0), and (1 1 3) family planes of the lithium niobate hexagonal phase [29]. The inset in **Figure 2(e)** shows a selected area electron diffraction pattern which confirms the existence of the hexagonal phase and the single-crystal nature of the LN particle shown in **Figure 1(e)**.

4. Conclusions

We described in detail the synthesis process of LN nanocrystals prepared by AACVD method, and we analyzed the effect of the most relevant parameters leading to nanocrystals taking a specific shape or size once they are synthesized. This has allowed us to demonstrate that it is possible to control the size and morphology of particles prepared adjusting the nucleation conditions. The synthesized nanocrystals showed different morphologies including quasi-cubic, tetrahedral, polyhedral, and hexagonal shapes, with characteristic sizes ranging from a few

tens to a few hundred nanometers. In addition to this, we also obtained rod-like structures with characteristic lengths ranging from 3 to 5 μm. The characterization of the prepared LN particles by GIXRD, SEM, and HRTEM techniques revealed the single-crystal nature of the synthesized particles.

Acknowledgements

The authors want to thank W. Antúnez-Flores, O. Solís, C. Ornelas-Gutiérrez, E. Guerrero, and J.T. Holguin, for experimental assistance, the Laboratorio Nacional de Nanotecnología and Centro de Investigación en Materiales Avanzados S.C. (CIMAV) for the facilities provided, and Ivan Rodríguez (Facultad de Filosofía y Letras, UACh, Universidad Autónoma de Chihuahua) for the assistance in the preparation of the chapter.

Conflict of interest

The authors declare no conflict of interest.

Abbreviations

LN	lithium niobate
AACVD	aerosol-assisted chemical vapor deposition
GIXRD	grazing incidence X-ray diffraction
SEM	scanning electron microscopy
HRTEM	high-resolution transmission electron microscopy

Author details

José G. Murillo[1*], José A. Ocón[2], Guillermo M. Herrera[3], José R. Murillo-Ochoa[4] and Gabriela Ocón[5]

1 Departmento de Física de Materiales, Centro de Investigación en Materiales Avanzados S. C., Chihuahua, Mexico

2 Universidad Tecnológica de Chihuahua, Chihuahua, Mexico

3 Cátedra CONACYT asignada al Departmento de Física de Materiales, Centro de Investigación en Materiales Avanzados S. C., Chihuahua Mexico

4 Universidad del Valle de Mexico, Chihuahua, Mexico

5 Universiadad Autónoma de Chihuahua, Chihuahua, Mexico

*Address all correspondence to: jose.murillo@cimav.edu.mx

References

[1] Arizmendi L. Photonic applications of lithium niobate crystals. Physica Status Solidi A: Applied Research. 2004;**201**:253-283

[2] Yim YS, Shin SY. Lithium niobate integrated-optic voltage sensor. Optics Communication. 1998;**152**:225-228

[3] Guarino A, Poberaj G, Rezzonico D, Degl'Innocenti R, Günter P. Electro-optically tunable microring resonators in lithium niobate. Nature Photonics. 2007;**1**:407-410

[4] Murillo JG, Herrera G, Vega-Rios A, Flores-Gallardo S, Duarte-Moller A, Castillo-Torres J. Effect of Zn doping on the photoluminescence properties of $LiNbO_3$ single crystals. Optical Materials. 2016;**62**:639-645

[5] Buse K, Adibi A, Psaltis D. Non-volatile holographic storage in doubly doped lithium niobate crystals. Nature. 1998;**393**:665-668

[6] Holm A, Stürzer Q, Xu Y, Weigel R. Investigation of surface acoustic waves on $LiNbO_3$, quartz, and $LiTaO_3$ by laser probing. Microelectronic Engineering. 1996;**31**:123-127

[7] Chang SJ, Tsai CL, Lin YB, Liu JF, Wang WS. Improved electrooptic modulator with ridge structure in x-cut $LiNbO_3$. Journal of Lightwave Technology. 1999;**17**:843-847

[8] Wooten EL, Kissa KM, Yi-Yan A, Murphy EJ, Lafaw DA, Hallemeier PF, et al. A review of lithium niobate modulators for fiber-optic communications systems. IEEE Journal of Selected Topics in Quantum Electronics. 2000;**6**:69-82

[9] Zhao L, Steinhart M, Yosef M, Lee SK, Schlecht S. Large-scale template-assisted growth of $LiNbO_3$ one-dimensional nanostructures for nano-sensors. Sensors and Actuators B: Chemical. 2005;**109**:86-90

[10] Guttmann E, Benke A, Gerth K, Böttcher H, Mehner E, Klein C, et al. Pyroelectrocatalytic disinfection using the pyroelectric effect of nano- and microcrystalline $LiNbO_3$ and $LiTaO_3$ particles. Journal of Physical Chemistry C. 2012;**116**:5383-5393

[11] Aufray M, Menuel S, Fort Y, Eschbach J, Rouxel D, Vincent B. New synthesis of nanosized niobium oxides and lithium niobate particles and their characterization by XPS analysis. Journal of Nanoscience and Nanotechnology. 2009;**9**:4780-4785

[12] Santulli AC, Zhou H, Berweger S, Raschke MB, Sutter E, Wong SS. Synthesis of single-crystalline one-dimensional $LiNbO_3$ nanowires. CrystEngComm. 2010;**12**:2675-2678

[13] Grigas AS, Kaskel S. Synthesis of $LiNbO_3$ nanoparticles in a mesoporous matrix. Beilstein Journal of Nanotechnology. 2011;**2**:28-33

[14] Cheng LQ, Li JF. A review on one dimensional perovskite nanocrystals for piezoelectric applications. Journal of Materiomics. 2016;**2**:25-36

[15] Boltersdorf J, King N, Maggard PA. Flux-mediated crystal growth of metal oxides: Synthetic tunability of particle morphologies, sizes, and surface features for photocatalysis research. CrystEngComm. 2015;**17**:2225-2241

[16] Wu N, Wang J, Tafen D, Wang H, Zheng J, Lewis JP, et al. Shape-enhanced photocatalytic activity of single-crystalline anatase TiO_2 (101) nanobelts. Journal of the American Chemical Society. 2010;**132**:6679-6685

[17] Zhu S, Zhang J, Qiao C, Tang S, Li Y, Yuan W, et al. Strongly

green-photoluminescent graphene quantum dots for bioimaging applications. Chemical Communications. 2011;**47**:6858-6860

[18] An C, Tang K, Wang C, Shen G, Jin Y, Qian Y. Characterization of $LiNbO_3$ nanocrystals prepared via a convenient hydrothermal route. Materials Research Bulletin. 2002;**37**:1791-1796

[19] Grange R, Choi JW, Hsieh CL, Pu Y, Magrez A, Smajda R, et al. Lithium niobate nanowires synthesis, optical properties, and manipulation. Applied Physics Letters. 2009;**95**:143105

[20] Wood BD, Mocanu V, Gates BD. Solution-phase synthesis of crystalline lithium niobate nanostructures. Advanced Materials. 2008;**20**:4552-4556

[21] Prakash BJ, Buddhudu S. Synthesis and characterization of Mn^{2+}: $LiNbO_3$ nano-particles by co-precipitation method. Indian Journal of Pure and Applied Physics. 2013;**51**:245-250

[22] Graça MPF, Prezas PR, Costa MM, Valente MA. Structural and dielectric characterization of $LiNbO_3$ nano-size powders obtained by Pechini method. Journal of Sol-Gel Science and Technology. 2012;**64**:78-85

[23] Mohanty D, Chaubey GS, Ourdkhani A, Adireddy S, Caruntu G, Wiley JB. Synthesis and piezoelectric response of cubic and spherical $LiNbO_3$ nanocrystals. RSC Advances. 2012;**2**:1913-1916

[24] Ocón JA, Murillo JG, Miki-Yoshida M, Cardoza MN, Contreras-López OE. Synthesis and characterization of $LiNbO_3$ nanocrystals prepared by the aerosol assisted chemical vapor deposition method. Journal of Crystal Growth. 2014;**408**:64-70

[25] Amezaga-Madrid P, Antunez-Flores W, Ledezma-Sillas JE, Murillo-Ramírez JG, Solís-Canto O, Vega-Becerra OE, et al. Synthesis, microstructural characterization and optical properties of undoped, V and Sc doped ZnO thin films. Journal of Alloys and Compounds. 2011;**509S**:S490

[26] Bornand V, Huet I, Bardeau JF, Chateigner D, Papet P. An alternative route for the synthesis of oriented $LiNbO_3$ thin films. Integrated Ferroelectrics. 2002;**43**:51-64

[27] Joshi DP, Pant G, Arora N, Nainwal S. Effect of solvents on morphology, magnetic and dielectric properties of (α-Fe_2O_3@SiO_2) core-shell nanoparticles. Heliyon. 2017;**3**:e00253

[28] Momma K, Izumi F. VESTA 3 for three-dimensional visualization of crystal, volumetric and morphology data. Journal of Applied Crystallography. 2011;**44**:1272-1276

[29] Joint Committee on Powder Diffraction Standards. Powder Diffraction File. card 01-070-8451. Swarthmore, PA: International Center for Diffraction Data; 2006